Predicting crack initiation in composite material systems due to a thermal expansion mismatch

E.S. FOLIAS[1], M. HOHN[1] and T. NICHOLAS[2]
[1]*Department of Mathematics, University of Utah, Salt Lake City UT 84112, USA; e-mail: folias@math.utah.edu*
[2]*Wright Laboratory Materials Directorate, Wright – Paterson Air Force Base, Ohio 45433-7817, USA*

Abstract. Residual stresses due to curing and thermal stresses due to differences between the thermal expansion coefficients of the matrix and fiber may have a major effect on the micro-stresses within a composite material system and must be added to the stresses induced by the external mechanical loads. Such microstresses are often sufficient to produce micro-cracking even in the absence of external loads, example during the cooling process.

In this investigation, a micro-mechnics approach is used in which the fibers of a composite material system are modeled as cylindrical inclusions that are embedded into a matrix plate. The model is then used to predict, analytically, the residual stresses due to a thermal expansion mismatch, e.g. during a cooling process. Additionally, some critical effects due to a load transverse to the direction of the fibers are examined. The analysis provides a better understanding of how residual stresses are developed and how they may be controlled in material systems where small strains are present.

Moreover, the results are used to identify locations of possible crack failure and to derive a fracture criterion for crack initiation at the local level. Comparison with experimental evidence for matrix cracking in intermetallic composites caused by thermal expansion mismatch shows a good agreement.

Key words: Residual stresses, thermal fracture, composites, micromechanics.

1. Introduction

In order to achieve revolutionary advances in turbopropulsion-powered systems for the next century, advanced high-temperature ceramic matrix composites will be required. Yet, fabrication of these advanced materials is still being accomplished by traditional trial-and-error approaches. Rarely such an approach, however, leads to an optimized material process that yields components of a high quality. Perhaps material modeling coupled with numerical simulation may be an intelligent approach to material processing which ultimately may lead to lower manufacturing costs.

Thus, if rational designs of ceramic composites are to be made, their performance under static, dynamic, thermally fatigued and environmental loads need to be predictable. The first step towards this goal is the realization that the ultimate failure, as well as many other aspects of the composite behavior, is the result of the growth and accumulation of microdamage to the fibers, matrix and their interfaces. Thus, it appears that any generally successful model of performance and failure must incorporate the effects of this damage at the microlevel. Coupling, therefore, between the micro-mechanical with that of the macro-mechanical behavior will be very helpful in developing rational methods for the prediction of the structural life span of such materials. This certainly represents a challenge.
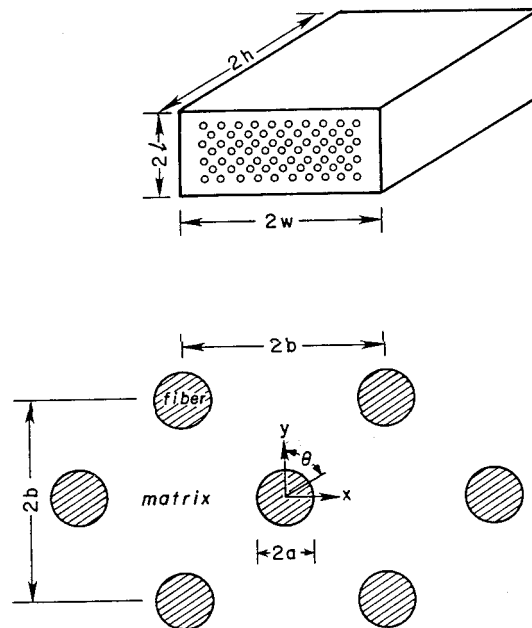
Figure 1.

For example, the residual stresses due to curing and thermal stresses due to differences between the thermal expansion coefficients of the matrix and fiber may have a major effect on the microstresses within a composite material system and must be added to the stresses induced by the external mechanical loads. Such microstresses are often sufficient to produce microcracking even in the absence of external loads, e.g. during the cooling process. Furthermore, if the material system is thermally fatigued, these residual stresses may cause some of the existing micro-cracks to grow and coalesce and thus form the presence of larger cracks.

In this investigation, a systematic 3D, micromechanics approach is used in which the fibers of a composite material system are modeled as cylindrical inclusions that are embedded into a matrix plate. The analytical model is then solved and the results are used to predict, the residual stresses due to a thermal expansion mismatch. The model provides a better understanding of how the residual stresses are being developed and how they may be controlled particularly in relation to ceramic materials where there is no ductility present to accommodate plastic deformation.

The analysis reveals the dependence of the residual stress field on the fiber volume fraction ratio, identifies the critical locations where a crack is most likely to initiate and subsequently propagate, recovers the interface shear stress profile and provides important information and guidance to material designers for the pre-selection of fiber and matrix materials in order to alleviate some of the residual stresses.

2. Mathematical model

Consider, for example, an infinite plate matrix which consists of material Beta21 (i.e. a titanium alloy), see Figure 1. The matrix plate is assumed to extend to infinity both in the x- and y-directions. In order to capture any possible 3D effects that may be present, the matrix plate

is assumed to have a finite dimension $2h$, along the z-direction. A uniform and square periodic arrangement of cylindrical fibers, for example SCS-6 (i.e. carbon-coated silicon carbide), is embedded into the matrix plate in the directions of the x- and y-axes. Although in the present study we are primarily interested in the residual stresses due to the thermal expansion mismatch, the material system is also vulnerable, in certain regions, to loadings that are transverse to the fibers. For this reason two different types of loads are being considered:

(i) a uniform temperature load ΔT (cooling) that is applied throughout the material system and

(ii) a uniform transverse load σ_0 perpendicular to the direction of the fibers and along the y-direction.

Such consideration will identify some of the critical locations of the material system that material designers should be aware of. Both fiber and matrix materials are assumed to be homogeneous and linearly elastic. While it is true that for this particular composite system the matrix is rather elastoplastic, in the present study we restrict the analysis to small strains. Moreover, this particular material system is used only as a vehicle to show some of the details of the model analysis.

The governing equations, are the well known Navier's equations coupled with the Energy Balance equation. More specifically,

$$\frac{1}{1-2\nu}\frac{\partial u}{\partial x} + \nabla^2 u - \frac{2(1+\nu)}{1-2\nu}\frac{\partial T}{\partial x} = 0, \tag{1}$$

$$\frac{1}{1-2\nu}\frac{\partial v}{\partial y} + \nabla^2 v - \frac{2(1+\nu)}{1-2\nu}\frac{\partial T}{\partial y} = 0, \tag{2}$$

$$\frac{1}{1-2\nu}\frac{\partial w}{\partial z} + \nabla^2 w - \frac{2(1+\nu)}{1-2\nu}\frac{\partial T}{\partial z} = 0, \tag{3}$$

$$\nabla^2 T = 0. \tag{4}$$

Where ∇^2 represents the Laplacian operator, T the temperature and ν Poison's ratio. The stress field can be obtained from the stress-strain equations:

$$\sigma_{ij} = \lambda \delta_{ij} \varepsilon_{kk} + 2G \varepsilon_{ij} - \alpha(3\lambda + 2G)(T - T_o)\delta_{ij}. \tag{5}$$

In this paper, $\Delta T = $ constant, which implies that all temperature derivatives with respect to space are zero.

As to boundary conditions, we require that:

(i) the appropriate stresses do vanish at the free edges, i.e.

$$\text{at } |z| = h, \qquad \sigma_{zz}^{(j)} = 0, \qquad \tau_{rz}^{(j)} = 0, \qquad \tau_{\theta z}^{(j)} = 0; \quad j = f, m \tag{6–8}$$

(ii) perfect bonding is assumed to prevail at the fiber/matrix interface, i.e.

$$\text{at } r = a, \qquad u_r^{(f)} = u_r^{(m)}, \qquad v_\theta^{(f)} = v_\theta^{(m)}, \qquad w^{(f)} = w^{(m)}, \tag{9–11}$$

$$\sigma_{rr}^{(f)} = \sigma_{rr}^{(m)}, \qquad \tau_{rz}^{(f)} = \tau_{rz}^{(m)}, \qquad \tau_{\theta r}^{(f)} = \tau_{\theta r}^{(m)}, \tag{12–14}$$
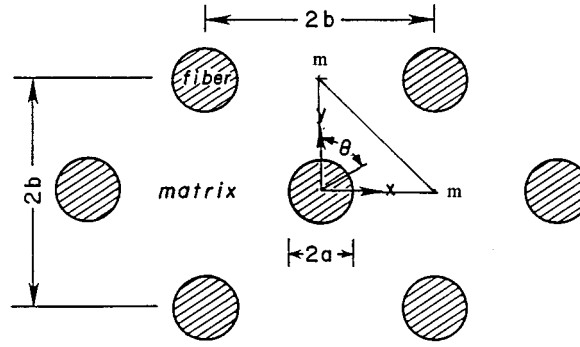
Figure 2. Cell configuration.

(iii) finally the boundary conditions within the cell configuration[1]. (See Figure 2), i.e. on the plane mm, $u_n^{(m)} = 0$, (15)

$$\tau_{mn}^{(m)} = 0, \qquad \tau_{mz}^{(m)} = 0, \qquad \int_{mm} F_x \, ds / A_{mm} = \sigma_0, \qquad \int_{mm} F_y \, ds = 0, \qquad (16\text{--}17)$$

where F_x, F_y are the resultant force components in the x- and y-direction respectively and A_{mm} the cross-sectional area of the plane mm. Moreover, the planes $x = 0$ and $y = 0$ are symmetry planes and, therefore, the solution must satisfy the symmetry boundary conditions.

3. The 3D displacement field

Without going into the mathematical details, the general 3D complementary displacement field satisfying boundary conditions (6–8) has already been constructed by Folias (1976) and the results may be expressed as:

$$u^{(c)(j)} = \frac{1}{m_j - 2} \sum_{\nu=1}^{\infty} \frac{\partial H_\nu^{(j)}}{\partial x} \{2(m_j - 1)f_1(\beta_\nu z) + m_j f_2(\beta_\nu z)\}$$

$$+ \sum_{n=1}^{\infty} \frac{\partial H_\nu^{(j)}}{\partial y} \cos(\alpha_n h) \cos(\alpha_n z) + l_1^{(j)} - y\frac{\partial l_3^{(j)}}{\partial x} + \frac{1}{m_j + 1} z^2 \frac{\partial^2 l_3^{(j)}}{\partial x \partial y}, \qquad (18)$$

$$v^{(c)(j)} = \frac{1}{m_j - 2} \sum_{\nu=1}^{\infty} \frac{\partial H_\nu^{(j)}}{\partial y} \{2(m_j - 1)f_1(\beta_\nu z) + m_j f_2(\beta_\nu z)\}$$

$$- \sum_{n=1}^{\infty} \frac{\partial H_n^{(j)}}{\partial x} \cos(\alpha_n h) \cos(\alpha_n z) + \frac{3m_j - 1}{m_j + 1} l_3^{(j)} + l_2^{(j)}$$

$$- y\frac{\partial l_3^{(j)}}{\partial y} - \frac{1}{m_j + 1} z^2 \frac{\partial^2 l_3^{(j)}}{\partial x^2}, \qquad (19)$$

---

[1] The reader should note that displacements are unique up to an additive constant.
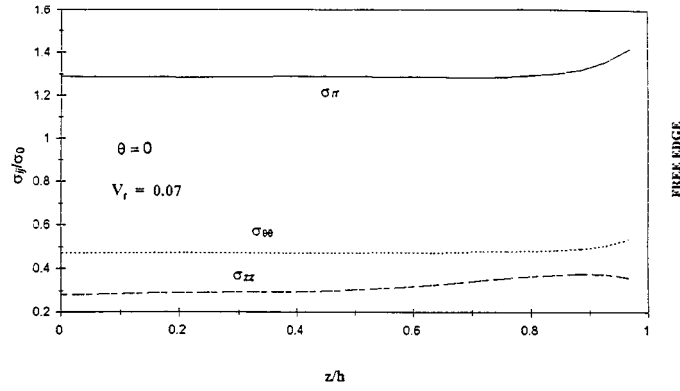
Figure 3a. Interface matrix stresses as a function of z/h and $a/h = 0.10$.
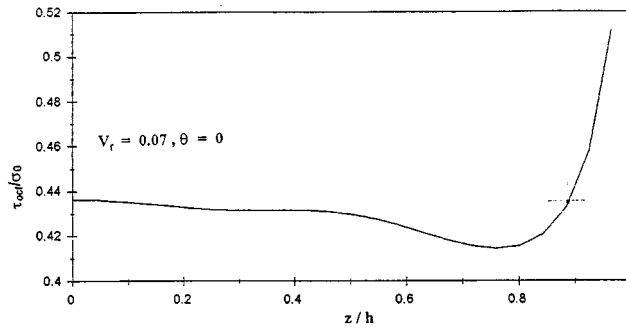

Figure 3b. Interface matrix octahedral shear stress as a function of z/h and $a/h = 0.10$.

$$w^{(c)(j)} = \frac{1}{m_j - 2} \sum_{v=1}^{\infty} \frac{\partial H_v^{(j)}}{\partial z} \{-2(m_j - 1) f_1(\beta_v z) + m_j f_2(\beta_v z)\}$$

$$-\frac{1}{m_j + 1} z \frac{\partial l_3^{(j)}}{\partial y}, \tag{20}$$

where $m = 1/v$, and

$$f_1(\beta_v z) = \cos(\beta_v h) \cos(\beta_v z), \tag{21}$$

$$f_2(\beta_v z) = (\beta_v h) \sin(\beta_v h) \cos(\beta_v z) - (\beta_v z) \cos(\beta_v h) \sin(\beta_v z), \tag{22}$$

$$\left(\frac{\partial^2}{\partial x^2} + \frac{\partial^2}{\partial y^2} - \beta_v^2 \right) H_v^{(j)} = 0, \tag{23}$$

$$\left(\frac{\partial^2}{\partial x^2} + \frac{\partial^2}{\partial y^2} - \alpha_n^2 \right) H_n^{(j)} = 0, \tag{24}$$

and where l_1, l_2, l_3 are 2D harmonic functions. Perhaps it is appropriate here to note that the displacement fields are expressed in terms of two infinite series the first of which has complex eigenvalues β_v, which are the roots of the equation

$$\sin(2\beta_v h) = -(2\beta_v h), \tag{25}$$

and complex eigenfunctions. The second series has real eigenvalues, $\alpha_n = n\pi/h$, $n = 1, 2 \ldots$, and real eigenfunctions. For more details of this form of the general solution see Penado and Folias (1989). Constructing next appropriate solutions to equations (23–24) in the polar form one has:

$$H_\nu^{(j)} = \sum_{k=0}^{\infty} \{A_k^{(j)} K_k(\beta_\nu r) + B_k^{(j)} I_k(\beta_\nu r)\} \exp(ik\theta) \qquad (26)$$

$$H_n^{(j)} = \sum_{k=0}^{\infty} \{C_k^{(j)} K_k(\alpha_n r) + D_k^{(j)} I_k(\alpha_n r)\} \exp(ik\theta) \qquad (27)$$

and for the 2D harmonic functions

$$l_l^{(j)} = \sum_{n=-\infty}^{\infty} \left\{ c_{nl}^{(j)} \left(\frac{r}{a}\right)^n + d_{nl}^{(j)} \left(\frac{r}{a}\right)^{-n} \right\} \exp(in\theta); \quad l = 1, 2, 3, \qquad (28)$$

where the constants $A_k^{(j)}$, $B_k^{(j)}$, $C_k^{(j)}$, $D_k^{(j)}$, $c_{nl}^{(j)}$, $d_{nl}^{(j)}$ are to be determined from the remaining boundary conditions (9–20). The reader should note that constants $A_k^{(j)}$, $B_k^{(j)}$ are complex.

Substituting the above equations into the remaining boundary conditions we arrive at a system of equations that are then used to solve for the unknown coefficients. Without going into the long and tedious numerical details, once the coefficients have been determined, the displacement and stress fields can then be recovered. For more details of the numerical approach, see Penado and Folias (1989).

4. Uniform loading transverse to the fibers ($\Delta T = 0$)

Although in the present study we are primarily interested in the residual stresses due to the thermal expansion mismatch, the material system is also vulnerable, in certain regions, to loadings that are transverse to the fibers in which case the effects may be even more pronounced. For this reason, we give some of the important results due to a transverse loading

(i) *Interior stress field*

For a constant transverse loading only along the direction of the x-axis (i.e. $\Delta T = 0$), the 3D stress field at the interface, for a volume fraction ratio of $V_f = 0.07$, was found to be constant all along the interior (see Figure 3(a)) and that as one approaches the free surface a boundary layer was observed to prevail, where the stresses increase rather rapidly. This suggests, therefore, that a stress singularity may be present in this region. It may also be noted that for fiber volume fractions of $V_f = 0.07$ or less, all interactions between fibers have for all practical purposes subsided.

There are four important 3D characteristics that one can draw from this figure. First, the width of this boundary layer is, approximately, two fiber diameters away from the free edge. Second, the amplitude of the stresses at the center of the fiber length is, in general, a function of the ratio of fiber diameter/fiber length. If, however, that ratio happens to be less than or equal to 1/10, then the magnitude of the stresses is precisely that of plane strain. Third, for ratios between 1/10 and 10 a state of 'pseudo plane strain' condition prevails whereby the amplitude
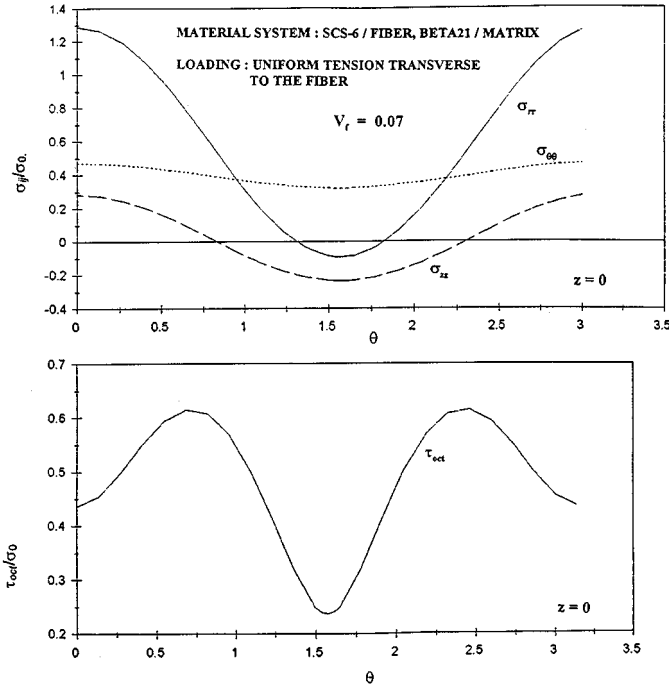
Figure 4. Interface matrix stresses on the plane $z = 0$ and as a function of θ.

of the stresses now increases, even on the plane $z = 0$, by as much as 10–12 percent. The term pseudo is used because away from the boundary layer, the condition

$$\sigma_{zz} = \nu(\sigma_{rr} + \sigma_{\theta\theta}) \tag{29}$$

is still satisfied even though the stresses are functions of the variable z. Fourth, for ratios greater than 10 the magnitude of the stresses is precisely that of plane stress. Finally, similar stress profiles exist for V_f ratios greater than 0.07, where the magnitude now is a function of V_f.

Figures 3(a,b) depict the profile of the interface stresses along the line $\theta = 0$ as a function of the ratio z/h. The numerical results are specialized for the material system: SCS-6/fibers, Beta21/matrix. Figures 4 and 5, show typical interface stress profiles of the matrix and fiber on the plane $z = 0$, and as functions of the angle θ.

(ii) *Edge stress field*

As it was previously noted, in the neighborhood of the free surface e.g. the edge of the plate or in the vicinity of crack bridging (see Figure 6), there may very well be present a stress singularity. By utilizing a local 3D asymptotic analysis one can substantiate the presence of a weak stress singularity. Complete details of this analysis can be found in the work of Folias (1989). Without going into the mathematical details, a summary of the results, for room temperature and for the material system discussed, is given below.

The local stress field is given by

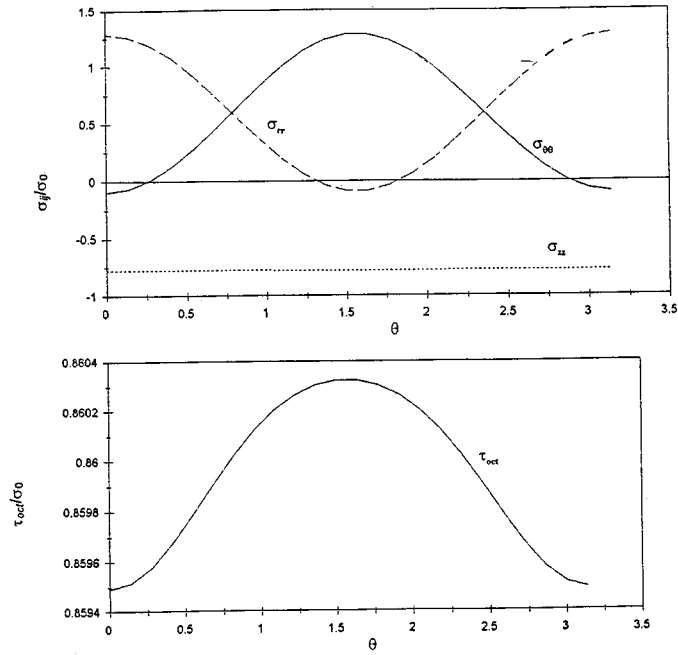$$\sigma_{ik}^{(j)} = \rho^{-\alpha} F_{ik}^{(j)}(\theta, \phi), \tag{30}$$

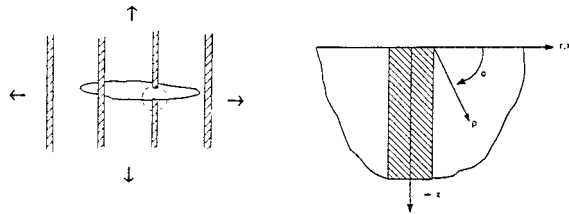*Figure 5.* Interface fiber stresses on the plane $z = 0$ and as a function of θ.

Figure 6. Fiber meeting a free surface.

where the $F_{ik}^{(j)}$ are explicit functions of the angles θ and ϕ and the stress singularity α is a function of the material constants. For a titanium matrix and SCS fibers it is found that

$$\alpha = 0.110 \ \text{at room temperature} \tag{31a}$$

$$\alpha = 0.190 \ \text{at} \ 900°C. \tag{31b}$$

While, in order to determine the residual stresses at room temperature it is only necessary to use the material constants of the system at room temperature, the material constants for 900°C were also used in order to see the difference of the stress singularity exponent α. The reader however, should be cautioned that this calculation is based on linear elasticity and on the presence of a constant temperature field.

Moreover, at $\phi = \frac{1}{2}\pi$ and for $G_f/G_m = 3.608$ it is found that

$$\sigma_{rr}^{(mm)} = -11.219\rho^{-\alpha} B^{(f)}, \tag{32a}$$

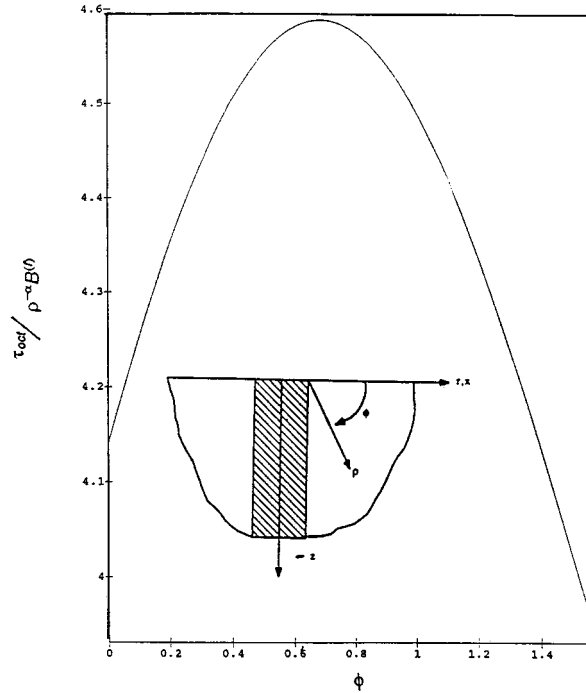$$\sigma_{\theta\theta}^{(mm)} = -4.823\rho^{-\alpha} B^{(f)}. \tag{32b}$$

Figure 7. The octahedral shear stress in the matrix and close to the edge where the fiber meets the free surface.

Similarly, at $\phi = 0$ it is found that

$$\sigma_{rr}^{(m)} = -9.970\rho^{-\alpha}B^{(f)}, \tag{33a}$$

$$\sigma_{\theta\theta}^{(m)} = -3.391\rho^{-\alpha}B^{(f)}, \tag{33b}$$

where $B^{(f)}$ stands for an arbitrary constant. The octahedral shear stress is plotted in Figure 7 where it is noted that its maximum occurs at $\theta = 40°$.

The following observations are also worthy of note. First, as the ratio of the shear moduli increases, so is the stress singularity. This is compatible with our physical expectations and within the assumptions of our theory. Second, all things being equal, at the edge the controlling stress for failure is the radial stress particularly at the location $\phi = 0$ and $\theta = 0$. Perhaps it is also appropriate here to note that the carbon coatings on the SCS-6 fibers produce a particularly weak interface. However, the authors would like to emphasize that this material system is only used as a vehicle to show how the details of this analysis work.

	Room Temp.	900°C
at $\phi = 0$:	$\dfrac{\sigma_{rr}^{(m)}}{\sigma_{\theta\theta}^{(m)}} = 2.94,$	$\dfrac{\sigma_{rr}^{(m)}}{\sigma_{\theta\theta}^{(m)}} = 2.94,$
at $\phi = \frac{1}{2}\pi$:	$\dfrac{\sigma_{rr}^{(m)}}{\sigma_{\theta\theta}^{(m)}} = 2.33,$	$\dfrac{\sigma_{rr}^{(m)}}{\sigma_{\theta\theta}^{(m)}} = 2.18.$

The reader may notice that there is a very small difference in the ratios.
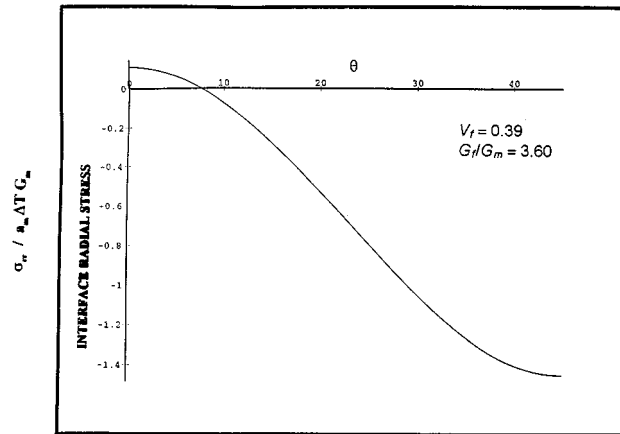
Figure 8. Interface radial matrix stress on the plane $z = 0$ and as a function of θ.

Similarly, in the vicinity of the edge, the octahedral shear stress attains a maximum at an angle of $\phi = 40°$ (see Figure 7). It is interesting to note that in this neighborhood, the ratio of

$$\frac{\tau_{octmax\,roomtemp}}{\tau_{octmax\,900C}} = \frac{1}{2.09}$$

which suggests that, at high temperatures, the material will undergo substantial plastic deformation in this region if subjected to a load transverse to the fibers.

Thus, a mode I and III crack failure may initiate at the edge and along the interface, particularly when the material system is subjected to a transverse (to the fibers) load in which case it becomes more pronounced.

5. Residual stresses due to ΔT ($\sigma_0 = 0$)

Residual stresses due to curing and thermal stresses due to differences between the thermal expansion coefficients of the matrix and fiber may have a major effect on the microstresses within a composite material system and must be added to the stresses induced by the external mechanical loads. Such microstresses are often sufficient to produce microcracking even in the absence of external mechanical loads, for example during a cooling process.

In this section we let the applied load $\sigma_0 = 0$ and furthermore assume ΔT to be a constant. The analytical model is then used to predict, the residual stresses due to the thermal expansion mismatch between the fiber and matrix.

Without going into the mathematical details, we consider a composite material system consisting of SCS-6 fibers which are embedded into a beta21 matrix plate and the entire system is then exposed to an environment of a uniform cooling temperature ΔT. While it is true that the material constants do change continuously as a function of the temperature, the thermal coefficients appear in the solution as a ratio, which ratio changes very little. On the other hand, the ratio of the shear moduli changes considerably as the temperature varies. Consequently, the results are very much dependent on the material properties which one uses. Thus, if one bases the analysis on the shear moduli ratio at room temperature, the following stress profiles are recovered at the fiber/matrix interface. Figure 8 depicts, for a $V_f = 0.39$, the radial matrix stress on the plane $z = 0$ and as function of the angle θ. It is noted that the radial
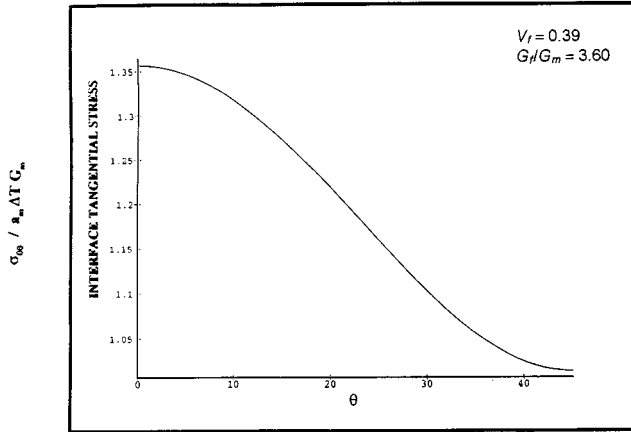
Figure 9. Interface $\sigma_{\theta\theta}$ matrix stress on the plane $z = 0$ and as a function of θ.

stress is compressive. Similarly, the tangential stress is tensile in nature and its maximum occurs at the location $\theta = 0$ (see Figure 9). In general, the location of this maximum is a function of the material properties and particularly of the shear moduli ratio. Moreover, in this analysis perfect bonding was assumed to prevail at the fiber/matrix interface. If, however, we were to relax the conditions at the interface whereby we allow slippage to occur, then the maximum will occur elsewhere. More specifically in this case it occurs at $\theta = 45°$.

Examining next the possibility of matrix cracking, it becomes evident from the above that no cracking will occur in the matrix for $\Delta T = 900°$C. This matrix material is too strong for preexisting microcracks to grow. Examination of the σ_{zz} stress also shows that no cracks will develop in that direction either. The results are in line with those obtained by Kroupa (1994) based on a finite element analysis.

Finally, it should be noted that the effect of the shear moduli ratio on the interface stresses can be substantial. This can be seen by the following comparison of the tangential interface stress when using three different shear moduli ratios that reflect three different and discrete temperature levels

V_f	$\dfrac{\sigma_{\theta\theta}}{\alpha_m G_m \Delta T}$	$\dfrac{\sigma_{\theta\theta}}{\alpha_m G_m \Delta T}$	$\dfrac{\sigma_{\theta\theta}}{\alpha_m G_m \Delta T}$
	Room Temp.	*Mid Temp.*	*High Temp.*
0.39	1.36	1.59	1.64

Although it would be desirable to have a program in which the material properties can vary continuously with temperature, one can compensate by taking the results corresponding to the high shear moduli ratio. The thermal expansion coefficients on the other hand appear as a ratio which ratio does not vary appreciably to make any significant differences.

The variation of the normalized tangential interface stress as a function of the fiber volume fraction for this material, is almost linear and may be approximated with the equation

$$\frac{\sigma_{\theta\theta}}{\alpha_m G_m \Delta T} = 0.92 + 1.02 V_f + 0.28 V_f^2. \tag{34}$$

In view of the above, this matrix will not exhibit any cracking as a result of the residual stresses which are developed during the cooling process. Experimental evidence showed no such cracking either.
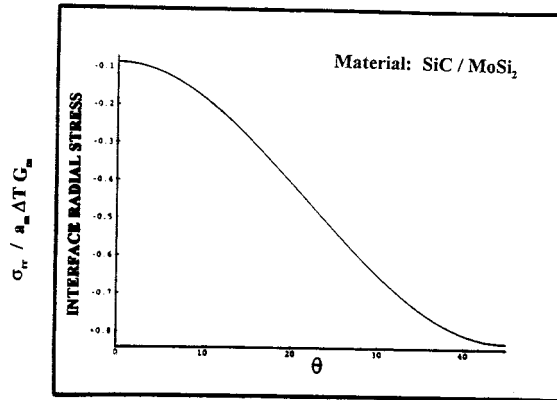
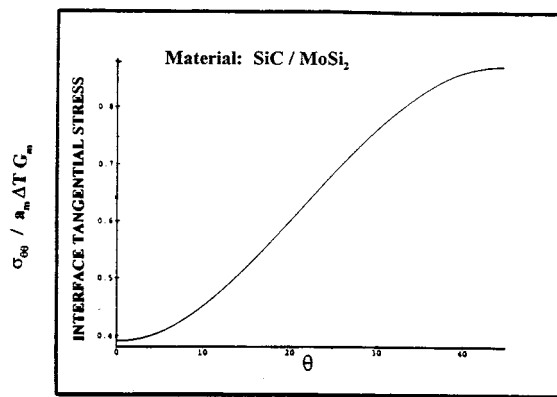*Figure 10.* Interface radial matrix stress on the plane $z = 0$ and as a function of θ.

Figure 11. Interface $\sigma_{\theta\theta}$ matrix stress on the plane $z = 0$ and as a function of θ.
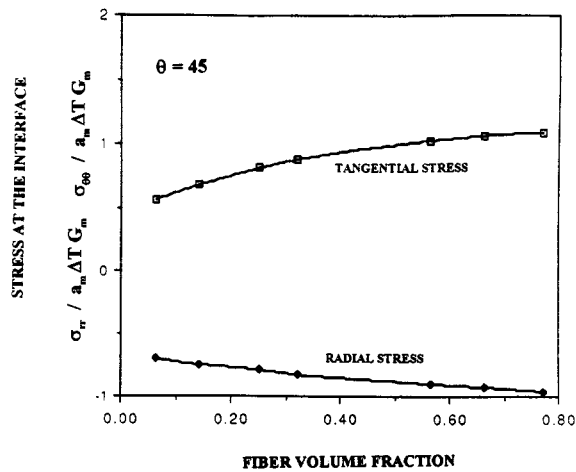

Figure 12. Normalized interface stresses on the plane $z = 0$ and as a function of V_f.

As a second physical example, we consider the material system consisting of SiC fibers embedded into an MoSi$_2$ matrix. The material system is characterized by the material properties $\nu_f = \nu_m = 0.25$, and $G_f/G_m = 1.05$, $\alpha_f/\alpha_m = 0.56$. Again omitting the mathematical details for a $V_f = 0.49$, the interface tangential, and radial stresses, on the plane $z = 0$ and as functions of the angle θ, are given in Figures 10–11, respectively. The reader may notice here that the maximum value of the tangential stress occurs at $\theta = 45°$, while the radial stress is compressive with a maximum absolute at $\theta = 0$. Finally, in Figure 12, we plot the variation of the maximum value of the tangential and radial stresses as a function of V_f. The following remarks are worthy of note

  (i) for a decrease in temperature (e.g. during cooling), $\sigma_{\theta\theta}$ is the controlling stress,
 (ii) for an increase in temperature (e.g. operating temperature), σ_{rr} is the controlling stress.

In general, the location of the maximum interface stress depends heavily on the material properties and not on the fiber spacing. This suggests, therefore, that all things being equal, during the cooling process a crack is most likely to develop at the interface and at $\theta = 45°$ and then advance into the matrix until it reaches the adjacent fiber. Alternatively, during the operating temperature the crack is most likely to develop along the interface and at $\theta = 0°$ and then advance along the interface towards the position $\theta = 45°$. Moreover, as the volume fraction ratio increases, the stresses increase in magnitude in the absolute value sense.

6. Fracture criterion for crack initiation

In view of our previous discussion, it is clear that the model may be used

  (i) to identify the location where cracks are most likely to initiate and propagate, and
 (ii) to identify the controlling stress that governs the failure.

Thus, if one assumes the presence of a small crack, of length c, in the matrix and adjacent to the interface, and along the direction of $\theta = 45°$, it is now possible to derive an approximate fracture criterion for crack initiation with which one can estimate the magnitude of the critical tangential stress that may cause the matrix to crack along this direction. More specifically (Hellan, 1984)

$$\{\sigma_{\theta\theta}^{(m)}\}_{\text{critical}} 1.12\sqrt{\pi c} \left\{ 1 - 0.15 \frac{c}{b\left(1 - \sqrt{2}\frac{a}{b}\right)} \right\} = K_c, \tag{35}$$

where K_c is the material fracture toughness and where

$$\{\sigma_{\theta\theta}^{(m)}\}_{\text{critical}} = \{\sigma_{\theta\theta}^{(m)}\}_{\theta=45°,\, r=a} \{\alpha_m \Delta T G_m\}, \tag{36}$$

of our previous analysis. Specializing the fracture criterion for the material system MoSi2/SIC one finds the critical cooling temperature T to be 1,356 Kelvin which corresponds to 1,083°C. In this case we assume a crack size of $c/a = 0.1$. The rational for this assumption is based not on a specific material but on previous knowledge of the behavior of 3D stress fields in regions where a boundary layer may be present as a result of an interface or a free boundary. Comparison with experimental observations carried out at Santa Barbara by Lu et al. (1992) on the same material system shows good agreement. The processing temperature reported was 1330°C, which is way beyond the critical value and for this reason cracks were expected
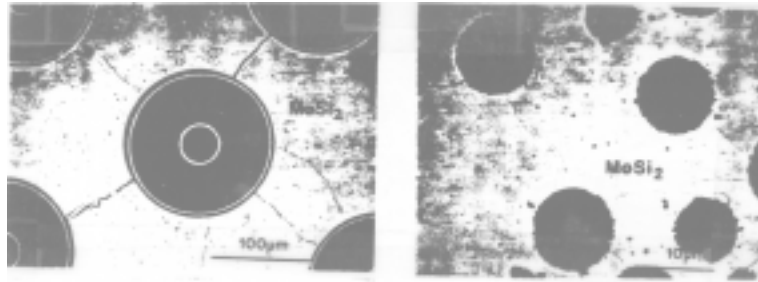
Figure 13. Experimental evidence of cracking in intermetallic composites.

to form, and they did (see Figure 13(a)). The model furthermore shows that, as the ratio V_f decreases, the magnitude of the residual stress also decreases and as a result the 'safe' cooling temperature increases to 1,197°C for a $V_f = 0.41$. Thus, the cracks in this case should be a little less visible, which they are (see Figure 13(b), where we have accounted for the different scale). Notice also that for this material system the cracks are at $\theta = 45°$, as predicted by the model. A similar criterion can also be developed for the radial, as well as the z-direction.

In conclusion, the model predicts an estimate of a safe processing temperature which will suppress the growth of microcracks. It may also be worthy to note that the theoretical model is applicable to ceramic, metal/matrix, as well as organic composites provided that the respective plastic deformations are relatively small. For moderately large plastic deformations, however, a correction factor to account for the nonelastic behavior of the matrix should be introduced.

7. Conclusions

An analytical model has been developed, in order to estimate the residual stresses for matrix cracking in ceramics and intermetalic composite material systems. The model may be used

- to identify the location where cracks are most likely to initiate and propagate, and
- to identify the controlling stress that governs the primary failure,
- to identify the controlling stress that governs the secondary failure,
- to provide information to material designers for the pre-selection of fiber and matrix materials.

Moreover, an approximate fracture criterion for crack initiation has been developed that may be used to predict the critical temperature, e.g. during the operating and cooling, beyond which micro-cracks are most likely to initiate and propagate within the material system. The criterion may also be used to search for possible optimization features between fiber spacing and material properties in order to achieve maximum strength.

Acknowledgments

References

Folias, E.S. (1975). On the three-dimensional theory of cracked plates. *Journal of Applied Mechanics* **42**, 663–674.

Folias, E.S. (1989). On the stress singularities at the intersection of a cylindrical inclusion with the free surface of a plate. *International Journal of Fracture* **39**, 25–34.

Hellan, K. (1984). *Introduction to Fracture Mechanics*, McGraw-Hill.

Isida, M. et al. (1991). Analysis of zig-zag array of circular inclusions in solid under uniaxial tension, *International Journal of Solids and Structures* **27**, 1515–1535.

Kroupa, J. (1994). Private communication.

Lu, T.C., Yang, J., Suo, Z., Evans, A.G., Hecht, R. and Mehrabian, R. (1992). Matrix cracking in intermetallic composites caused by thermal expansion mismatch.

Penado, E. and Folias, E. S. (1989). The three-dimensional stress field around a cylindrical inclusion in a plate of arbitrary thickness, *International Journal of Fracture* **39**, 129–146.